VALIDATION OF RING FILAMENT WOUND FIBER PATHS FOR UNIDIRECTIONAL PREFORM PLY MANUFACTURING

F. A. Finkenwerder[1], M. Geistbeck[2] and P. Middendorf[3]

[1]Airbus Group Innovations, Composite Technologies, Airbus Group,
Willy-Messerschmitt-Strasse 1, 81663 München, Germany
Email: felipe.finkenwerder@airbus.com, Web Page: http://www.airbus-group.com
[2]Airbus Group Innovations, Composite Technologies, Airbus Group,
Willy-Messerschmitt-Strasse 1, 81663 München, Germany
Email: matthias.geistbeck@airbus.com, Web Page: http://www. airbus-group.com
[3]Institute of Aircraft Design (IFB), University of Stuttgart,
Pfaffenwaldring 31, 70569 Stuttgart, Germany
Email: peter.middendorf@ifb.uni-stuttgart.com, Web Page: http://www.ifb.uni-stuttgart.com

Keywords: filament winding, validation, unidirectional, non-geodesic, preform

Abstract
Contrary to conventional filament winding methods, ring filament winding enables to process continuous fibers for the manufacture of unidirectional, non-crimp preform plies on curved and closed mandrel geometries. The winding motion here is realized by a ring shaped configuration of a fiber supply unit, instead of a rotating mandrel. The objective of the present study is to validate geodesic and non-geodesic trajectories at room temperature conditions by unidirectional ring filament winding. Preliminary experiments have identified the magnitude of tow tensile force and its dependency from the take-up velocity. Validation experiments of geodesic winding paths investigate the reproducibility of winding angles by variation of the tow tensile force and the take-off velocity. Results show a good agreement with analytical data and a high reproducibility for angles ranging from 15° to 85°. Non-geodesic winding experiments investigate the reproducibility of fiber paths by variation of the winding method, the slippage coefficient and the mandrel surface material. Results highlight a range, where lateral tape slippage occurs and the dependence of the coefficient of friction from the correlation between the tensile force and the take-off velocity.

1. Introduction
Filament winding is a state of the art manufacturing technology for straight formed composite parts, e. g. profiled beams and pressure vessels. High material deposition rates plus the possibility of online processing thermoset or thermoplastic matrix systems are typical advantages, which enables profitability and tailoring part properties. Therefore online processing strategies, characterization of filament wound laminate properties as well as novel machine configurations, have been extensively studied [1]–[3]. However, the winding principle based on a continuous rotation of mandrel along its longitudinal axis, was kept the same. Different machine configurations, which typically consist of four axis system, have been developed to continuously process multiple fiber bundles [4]. The processing of a single filament wound pattern is originated from repeatedly winding the same fiber angle next to each other after every mandrel revolution. Consequently, a complete pattern is composed by a multiple times self-intersecting single tow. Beside of all the described advantages, it is known that fiber undulations lead to a laminate's loss of strength [5]. A further significant process disadvantage is the high machine complexity required to produce restricted part geometries. Both restrictions disqualify the process for possible applications in aerospace industry. Ring filament winding technique is based on a novel configuration of a fiber supply unit in form of a ring, which consists of an integrated fiber bobbin and a guidance device. The winding motion is performed through constant ring rotation.

Excerpt from ISBN 978-3-00-053387-7

Coupling it to a feed unit (e. g. a robot or a linear axis) a customization of fiber trajectories in different angles is enabled. This concentration of feed and winding motion in one unit eliminates the necessary rotation of the mandrel around its longitudinal axis and opens the possibility to process mandrel shapes in curved and/or closed geometry. In this context, fiber trajectories can be processed without crimps and with increased angle variability for manufacturing of an unidirectional preform ply.
Ring filament winding, e. g. toroidal filament winding, has been first investigated numerically by Zu et al. [6], [7]. Optimization of mechanical properties, design and analysis possible geodesic and non-geodesic fiber trajectories for toroidal pressure vessels were investigated, verifying results with mechanical testing. Zu stated that non-geodesic fiber paths not only fulfill geometry requirements for a whole unidirectional pattern, but also significantly contribute to a mass reduction aligning fiber paths along load directions. Schädel et al. studied ring filament winding experimentally, as a joining method for space-frame T-Joint intersections [8]. Mechanical characterization shows achievable fraction forces up to 50 kN before T-joint's failure.

2. Objective

The focus of the present study is to validate geodesic and non-geodesic trajectories at room temperature conditions, by unidirectional ring filament winding. Winding angles and its reproducibility for both kinds of fiber trajectories have been investigated through variation of multiple parameters, such as tow tensile force, take-off speed, winding method, slippage coefficients and the mandrel's substrate material. In this context, analytical calculations are compared do empirical data for geodesic and non-geodesic fiber trajectories. Measurement of process forces at the nip-point and of the angle variation along fiber trajectories characterize tow lateral slippage and define a scope, within which the effect does not occur. A projection of the process boundaries is trailed targeting multiple preform ply manufacturing for aeronautic applications.

3. Analytic and Experimental Procedure

3.1. Analytics

Geodesic trajectories are described by the law of Clairaut [9] and affirm, that the geodesic curvature is equal to zero. Specifically, for a cylindrical straight mandrel, it is therefore estimated by the angle dependent take-off velocity v_t. The take-off velocity is calculated through a given the rotational velocity n_0 of the winding ring, the winding angle α and the feed rate v_f of the mandrel Equation (1).

$$v_t = \sqrt{{n_0}^2 + {v_f}^2} = n_0 \cdot \sqrt{1 + \frac{1}{(\tan\alpha)^2}} \tag{1}$$

Clairaut's non-geodesic trajectories are hence characterized by a geodesic curvature of the winding path unequal to zero. The geodesic curvature κ_G, is described through the ratio of the winding angles gradient between two discretization units along the fiber pathway. The normal curvature κ_N is directly dependent of the winding angle α and the mandrels cross-sectional radius r_m. The ratio between the geodesic curvature and the normal curvature of a winding path determinates the slippage coefficient λ, shown in Equation (2) [9].

$$\kappa_G = \frac{\Delta\alpha}{\Delta s}; \kappa_N = \frac{(\sin\alpha)^2}{r_m}; \lambda = \frac{F_s}{F_n} = \frac{\kappa_G}{\kappa_N} \tag{2}$$

The slippage coefficient λ is also proportional to the ratio of tow's lateral by the normal force. Therefore, λ is stated as an introduced mathematical variable, for designing non-geodesic winding pathways. An equivalent variable is the coefficient of friction μ, which is described by Coulomb's friction law and is a physical measurement of the friction between two sliding material counterfaces. Couloumb's coefficient of friction is estimated by dividing friction load through the normal (constant) load [10]. In cases of a variating normal load, Howell's equation of friction can be expressed in terms of Couloumb [10]. Thus the inequality of the slippage coefficient and the coefficient of friction defines if and when side tow slippage physically occurs [11]. Normal force F_n and lateral force F_s can be determined through specifying the value of tow tensile force F_t for a given winding angle. Consequently the tow's lateral force F_s is calculated with Equation (3), by multiplication of λ with F_n.

Excerpt from ISBN 978-3-00-053387-7

An illustration of the process forces at the nip-point while filament winding is given by Figure 1(B), where w_T refers to the tape width.

$$F_n = \frac{(\sin\alpha)^2 \cdot F_t \cdot w_T}{r_m}; F_s = \lambda \cdot F_n; \quad (3)$$

3.2. Experimental Procedure

The test rig for ring filament winding consists of a six-axis robotic arm with an integrated Schunk FTD-Delta force-toque sensor, a winding ring and an asynchronous electrical motor. The robotic arm has the function to carry and position the mandrel horizontally, enabling feed rates to be programed by discretization of the winding trajectories in 20 units. The winding ring is equipped with a seven element tow guidance system, a bobbin carrier and a hysteresis brake Mobac 655KH. Figure 1(A) illustrates the configuration of the ring filament winding test rig. A cylindrical mandrel, with a 120 mm round profile, have been selected for the conduction of experiments. It represents the simplest mandrel design and nevertheless permits an easy implementation and evaluation of winding trajectories enabling to assign results onto more complex geometries, e. g. curved mandrels. For the suggested parameter investigation, the mandrel's surface is prepared with two textiles. Such an approach offers a defined and reproducible surface topology for the winding tests. On the other hand, process-relevant conditions might be illustrated. The selected textile materials are (a) a plain weave peel ply fabric with polyester filaments and (b) 12k IM carbon fiber tapes, in 5 mm width, bindered with a thermoplastic fleece. Due to non-disclosure agreements, material labels are kept anonymized. A peel ply substrate sets an analogy to process conditions for the first preform ply, whereas a carbon fiber substrate assign conditions for all following preform plies. Peel ply's warp direction is fixed in longitudinal direction of the mandrel. For the mandrel surface preparation using carbon fiber tapes, hoop winding method is applied, so that the filaments are angled approximately to the circumference direction. At room temperature conditions the thermoplastic fleece is held under its glass transition temperature, having therefore no adhesive effect. Moreover, a constant tape width has the particularly advantage to process single preform ply with a constant areal weight, supporting a high lay-up quality. In first validation experiments geodesic winding paths are performed. The interaction between winding angle, tow tensile force and take-off velocity is investigated applying a helical winding method. Since geodesic trajectories are not sensitive on lateral slippage, a mandrel surface with prepared plain weave peel ply coverage is used. A Design-of-Experiments CCD-Plan is applied to simplified experimental efforts repeating every point at least three times. A quantitative measurement of the accordance quality between analytical and experimental results is given by the correlation coefficient R^2.

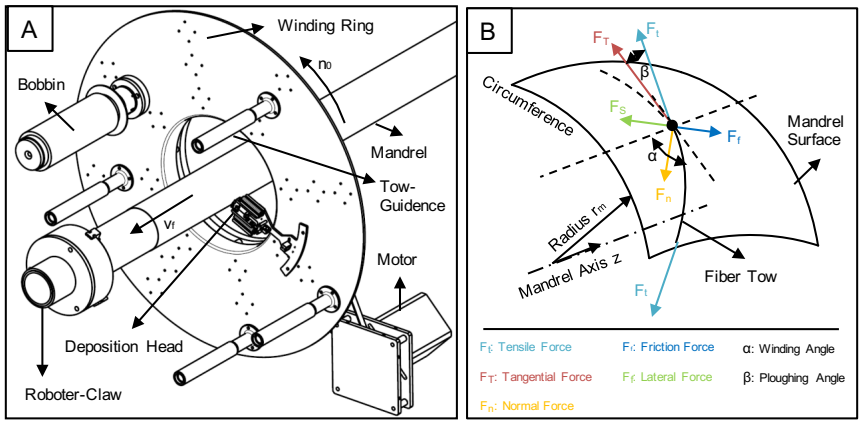

Figure 1. The ring filament winding test rig with its corresponding component is shown in (A). A qualitative illustration of process forces vectorization at the nip-point is illustrated in (B).

The second part of validation experiments deals with the validation of non-geodesic winding paths, setting three parameters to be parameterized: (a) slippage coefficient, (b) mandrels coverage material

Excerpt from ISBN 978-3-00-053387-7

and (c) the winding method. The bobbin's break torque is set constant at 25% for a starting tow tensile force. A range of coefficient of friction is determined evaluating the coordinates, at which the tape has sticked to the mandrels surface. To illustrate a helical- and parallel-helical winding methods, two different kind of path have been planned: a „S"- and an „O"-shaped continuous non-geodesic path. An S-shaped path is characterized at first by an increasing angle, starting from the pre-defined angle α_0=50°, until α=90°, followed then by a decrease back to α_0=50°. The respective feed rate has its values differentiated, while its direction is kept forward. An O-shaped path is characterized the same as the „S" one until α=90° is reached. Afterwards the feed rate reverses its direction backwards, creating a symmetric pathway to the forward one. Non-geodesic fiber paths are created by discretization of the feed rate in 20 units, keeping the number of revolutions of the winding ring constant. Take-off velocity is set starting at 137,2 mm/s (at α_0=50°) and being decreased to 30 mm/s (α=90°). This means that the maximum achievable coefficients of friction are directly correlated to the minimum take-off velocity at α=90°. Due to the lower number of parameters a full factorial design is applied. Table 1 presents the summarized experimental plans for geodesic and non-geodetic tests.

Table 1. Parameters of geodesic winding experiments based on a DoE-CCD-Plan and those of non-geodesic winding experiments on a DoE-full factorial-design.

Geodesic Filament Winding					
α (°)	15	29,1	50	70,8	85
F_t (N)	7	10,65	16	21,35	25
v_t (mm/s)	30	73,5	137,2	201	244,5

Non-Geodesic Filament Winding			
Material	Peel Ply		12k IM CF
Winding Method	O-Shape		S-Shape
λ (-)	0,3	0,5	0,7

Process force vectors at the nip-point are first calculated analytically and then compared to experimental data. Tape lateral and normal forces are evaluated by taking an imprint of the sticked trajectory on a transparent foil and following evaluation with a self-written Matlab-algorithm. Error tolerances are limited within ±0,5 mm relative to the picture scaling from pixels to millimeters.

4. Results and Discussion

4.1. Influence of tow take-off velocity on tensile force F_t

The characterization of the tensile force magnitude in dependence of the take-off velocity is performed variating brake torque into 0, 12,5, 25, 37,5 and 50%. The tow's take-off velocity was combined to each level systematically by a five level regular discretization between 30 mm/s and 244,5 mm/s. Results illustrated in Figure 2 highlight an increase of the tensile force with increasing take-off velocity from 4,7 N (30 mm/s) to 25 N (244,5 mm/s). Geodesic winding experiments investigate the whole range of the tensile force. For non-geodesic winding experiments, the tensile force is delimited from 13 N to about 10 N, since the take-off velocity decreases from 137,2 mm/s to 30 mm/s.

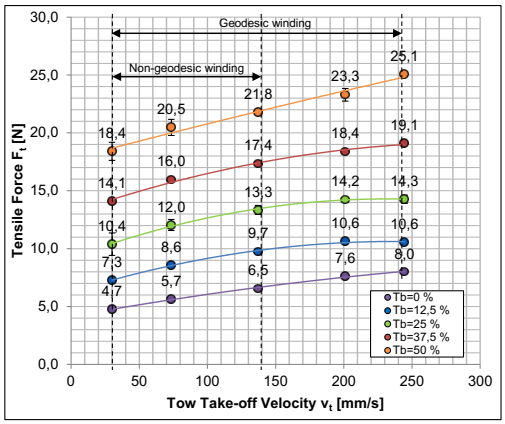

Figure 2. Tow's tensile force measurements in denpendence of the brake torque and take-off velocity.

Excerpt from ISBN 978-3-00-053387-7

4.2. Validation of geodesic winding paths

An overview of angle measurement results from geodesic pathways is presented in Figure 3(A), by comparing analytical with experimentally measured angles. For geodesic winding angles between 15° and 85°, R^2 is 0,99 and confirms a high reproducibility of the process under this conditions. Over all investigated scope, standard deviations does not exceed ±5 %. Moreover it can be noticed, that windings angles in the range between 15° until 29° are more sensitive to deviations than other angles. Although an exact angle limit cannot be strictly discerned, upon which angle deviations are minimal, the increase of an unstable behavior for geodetic winding paths explained by means of the correlation of take-off velocity with normal force vectors. This correlation effects are illustrated in Figure 3(B). A visible higher discrepancy of the winding angle (purple dots), within this given range, is rather correlated with deviations of the tow tensile force(blue dots) at 73,5 mm/s, than at higher take-off velocities. This effect is associated to the path's reduced normal curvature for lower winding angles, leading to higher a sensitivity of the tape to fluctuation of the circumference force vector. These fluctuations can be associated to the manual set up of the bobbin's brake torque, but also to variation of the unwinding angle at lower take-off velocities, which has been observed in previous tests. Hence a reasonable compromise is to either set tensile forces below 10 N or to wind with higher take-off velocities. Investigations of non-geodesic winding paths are executed accordingly.

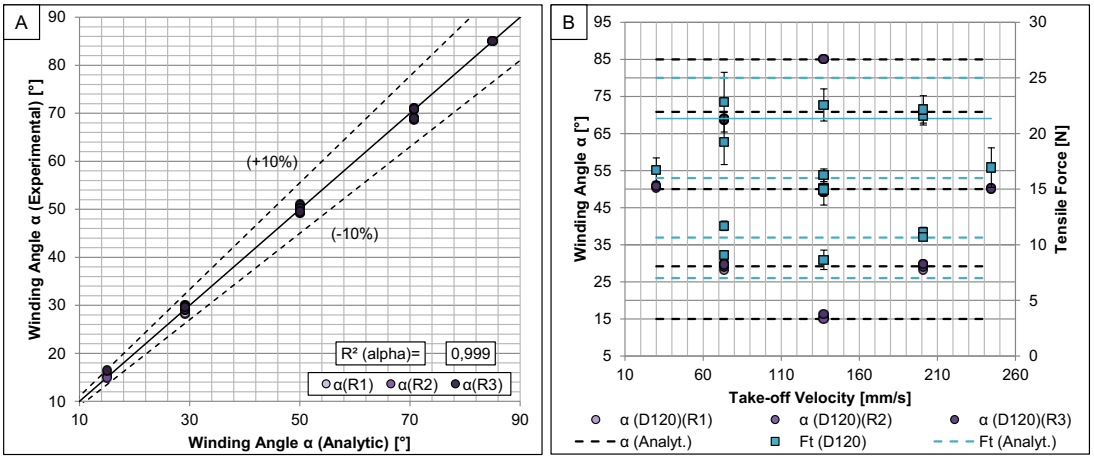

Figure 3. Analytic and experimental winding angles are compared in (A). The influence of tensile force and fiber take-off velocity on resulting winding angles are illustrated in (B).

4.3. Validation of non-geodesic winding paths

4.3.1 O-Shaped winding path

Experimental results of O-shaped non-geodesic winding paths confirm lateral slippage for both investigated mandrel surface materials, being mainly differentiated by its tolerance fields. A higher stick behavior and tighter tolerances are observed at trajectories performed on hoop wound carbon fiber substrates. Non-geodesic trajectories for λ=0,3 performed on plain weaved peel ply, sticked around a -30 % tolerance field, while paths associated to λ=0,5 turn out to be limited at a -20 %. Normally the opposite result would be expected. An effect of tape side inclination on the mandrel's surface is observed by winding λ=0,5 pathways and seams to explain this differences. The increase of the geodesic curvature κ_G combined with tendentially decreasing tensile forces generate a tensile force gradient along the tape width, causing tape side inclination. An intensification of this effect is observed for winding paths layed-up on a hoop wound carbon fiber surface. In this case, O-shaped pathways with λ=0,3 are limited to -30 % tolerances, while paths with λ=0,5 reach even a -10 %, due to tape sided inclination. A general explanation to the higher accordance of fiber pathways with λ=0,5 to analytics, compared to pathways with λ=0,3, is attributed to the reduced contact between the tape's and the mandrel's surface. This leads to an increase of normal pressure and consequently to an increase of the coefficient of friction, independently of the material pairing. The observed influence of

Excerpt from ISBN 978-3-00-053387-7

the normal pressure on stick-slip-behavior corresponds to conclusions of [10] considering the friction between dry carbon fibers. The intensification of this effect regarding winding trajectories on a hoop wound carbon fiber substrate is rather attributed to the rougher surface topology, compared to a plain weaved polyester peel ply.
Figure 4(A) outlines differences between analytical and experimental O-shaped non-geodesic winding trajectories quantitatively, for a slippage coefficient of λ =0,5 on a hoop wound carbon fiber surface. Dots assign a three time repetition of experimental experiments respectively, while continuous lines are related to analytics. Dashed lines represent tolerance fields and support the characterization of stick-intervals. A comparison between analytical and experimental winding angle deviations is illustrated in Figure 4(B). Analysis of winding angles indicate not only the low slippage tendency, but also confirms a higher reproducibility for a hoop wound carbon fiber sbstrate. Lateral slippage is restricted to widening deviations of the winding path of $\Delta\alpha=\pm5°$, measured before and after the $\alpha=90°$ mark is reached. In Figure 4(C) normal and lateral force measurements are illustrated, showing mostly good agreement with analytics. In Figure 5(A) analytical slippage coefficients (in color patterns) are compared to resulting coefficients of friction (in black patterns) out of O-shaped winding paths. An average coefficient of friction among the carbon fiber tape with polyester peel ply counterfaces is restricted to $\mu=0,31$, whereas for a hoop wound carbon fiber substrate it reaches $\mu=0,49$.
It can be resumed, that O-shaped non-geodesic trajectories could not be fully validated compared to analytics. Additionally, it was noticed that there is a tendency of the coefficient of friction to increase with increasing normal pressure at the nip-point. The reason for this effect is the greater interlocking effect between tow and the substrate filaments, being intensified due to a rougher surface topology. The influence of the variation of the tensile forces with the take-off velocity on the reproducibility of non-geodesic winding trajectories is not part of the study. The determined limits for the coefficient of friction provide thus just a preliminary trend for designing non-geodesic fiber trajectories.

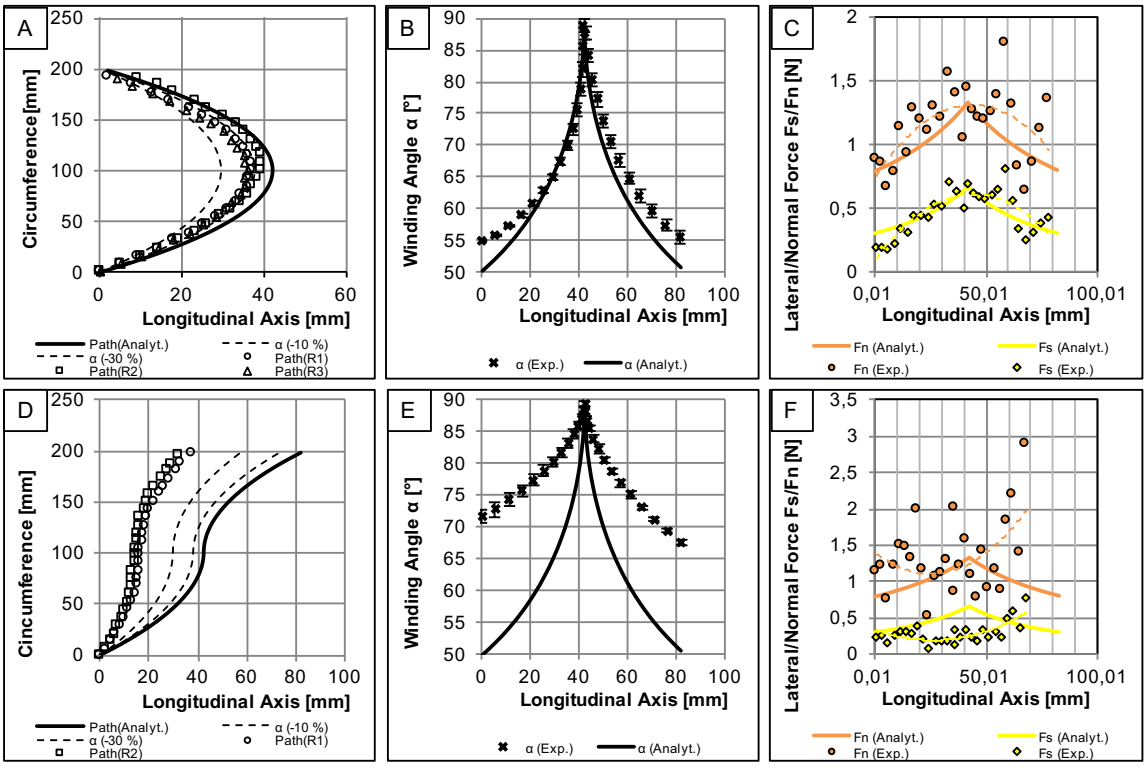

Figure 4. Comparison of experimental and analytical O-shaped (A) and S-shaped (D) non-geodesic fiber paths for λ=0,5 on a hoop wound mandrel surface.Their corresponding angle courses are shown in (B) and (E). Normal and lateral force responses are illustrated in (C) and (F).

Excerpt from ISBN 978-3-00-053387-7

4.3.2 S-Shaped winding path

Experimental results for S-shaped winding paths show an increased slippage behavior than those of O-shaped paths. A direct comparison between pathways, angles and process forces among an O-shaped path is summarized in Figure 4. After a two-step repetition of the slippage coefficient, an average of λ=0,3 pathways sticks at a -30 % tolerance of the analytical path, for both substrate materials. This suggests that a small proportion of lateral slipping occurred already before an angle of 90°, shifting the whole pathway against mandrel's feed direction. Angle deviations stay within ±10 % compared to analytics, achieving an average minimum of α=52°. Fiber trajectories for λ=0,5 and λ=0,7 demonstrate an even higher slippage tendency compared to λ=0,3, reaching a minimum winding angle of only α=70°. Within this scope, the influence of stick-slip-behavior [12] is noticed to be the reason for elevated standard deviations and reduced reproducibility.

To illustrate slippage behavior, Figure 4(D) shows S-shaped non-geodesic winding paths performed on a hoop wound carbon fiber mandrel surface for λ=0,5. The respective path angle response is shown in Figure 4(E). Interesting is, that for all S-shaped fiber trajectories tape side inclination is not observed. The drop in normal pressure through the fully contact of the tape's width at the nip-point leads to lower coefficients of friction in comparison to O-shaped pathways (Figure 5). Factors which contribute to minimize tape side inclination are: the maintenance of the feed rate direction, the minor geodesic curvature at λ=0,3 and the increased tape slippage at λ=0,5 und λ=0,7. Normal and lateral force responses, ploted in Figure 4(F), evidence a higher slippage behavior through the accentuated drop of lateral forces. This confirms the accentuated normal pressure dependency of the coefficients of friction and point it out as a reason for the high slippage tendancy. Since the interaction of the tensile force with the the take-off velocity have not been varied for non-geodesic experiments, the resulting coefficients of friction are considered as preliminary but not as absolute values. Optical evaluation of the sticked winding paths points out a maximum average friction coefficient of only μ=0,35 for both substrates (Figure 5) (B).

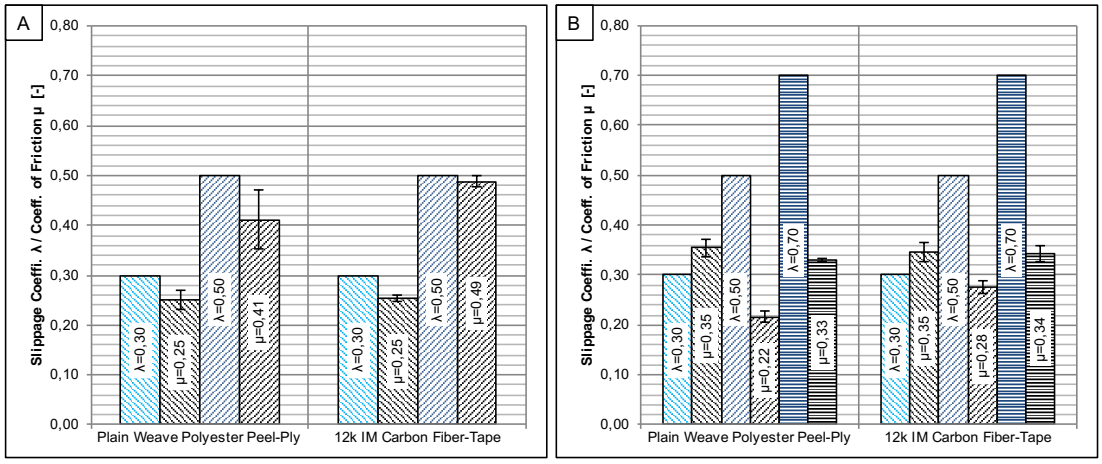

Figure 5. Comparison of coefficients of friction μ with the set up slippage coefficients λ for O-shaped (A) and S-shaped (B) non-geodesic pathways, on a peel ply and a hoop wound carbon fiber substrate.

5. Conclusion

Ring filament winding has been experimentally validated for geodesic fiber trajectories, achieving high reproducibility with accordance to analytics. Findings outline a higher reproducibility with increasing fiber take-off velocity (up to 244,5 mm/s), enabling to design the process in a profit orientated point of view. Non-geodesic winding trajectories were successfully implemented experimentally in an O- and S-shape, but could not be fully validated to analytics. Results have shown higher deviations of the pathways to analytics because of lateral tow slippage. A substancial dependency of the coefficient of friction from normal pressure, process velocity and the material's

Excerpt from ISBN 978-3-00-053387-7

surface topology at the nip-point was noticed to determine stick-slip-behavior. Finally, only preliminary limits of the coefficient of friction could be assigned for each winding method.

References

[1] J. Romagna, G. Ziegmann, and M. Flemming, "Thermoplastic filament winding-an experimental investigation of the on-line consolidation of poly(ether imide) fit preforms," *Compos. Manuf.*, vol. 6, no. 3–4, pp. 205–210, 1995.

[2] D. Cohen, "Influence of filament winding parameters on composite vessel quality and strength," *Compos. Part A Appl. Sci. Manuf.*, vol. 28, no. 12, pp. 1035–1047, 1997.

[3] P. Mertiny and F. Ellyin, "Influence of the filament winding tension on physical and mechanical properties of reinforced composites," *Compos. Part A Appl. Sci. Manuf.*, vol. 33, no. 12, pp. 1615–1622, 2002.

[4] R. Schledjewski and M. Päßler, "Filament winding with increased efficiency," no. Institut für Verbundwerkstoffe GmbH, Kaiserslautern, Germany, www.ivw.uni-kl.de, pp. 1–6, 2012.

[5] O. Meyer, "Kurzfaser-Preform-Technologie zur kraftflussgerechten Herstellung von Faserverbundbauteilen," *Diss. Fak. Luft- und Raumfahrttechnik und Geodäsie der Univ. Stuttgart*, 2008.

[6] L. Zu, S. Koussios, and A. Beukers, "Shape optimization of filament wound articulated pressure vessels based on non-geodesic trajectories," *Compos. Struct.*, vol. 92, no. 2, pp. 339–346, 2010.

[7] L. Zu, D. Zhang, Y. Xu, and D. Xiao, "Integral design and simulation of composite toroidal hydrogen storage tanks," *Int. J. Hydrogen Energy*, vol. 37, no. 1, pp. 1027–1036, 2012.

[8] J. Fleischer and J. Schaedel, "Joining automotive space frame structures by filament winding," *CIRP J. Manuf. Sci. Technol.*, vol. 6, no. 2, pp. 98–101, 2013.

[9] J. Romagna, "Strategien in der Faserwickeltechnik," *Dissertation;*, vol. Eidgenössi, no. 12450, p. 308, 1997.

[10] B. Cornelissen, B. Rietman, and R. Akkerman, "Frictional behaviour of high performance fibrous tows: Friction experiments," *Compos. Part A Appl. Sci. Manuf.*, vol. 44, no. 1, pp. 95–104, 2013.

[11] R. Wang, W. Jiao, W. Liu, F. Yang, and X. He, "Slippage coefficient measurement for non-geodesic filament-winding process," *Compos. Part A Appl. Sci. Manuf.*, vol. 42, no. 3, pp. 303–309, 2011.

[12] C. Gao, D. Kuhlmann-Wilsdorf, and D. D. Makel, "Fundamentals of stick-slip," *Wear*, vol. 162–164, no. PART B, pp. 1139–1149, 1993

Excerpt from ISBN 978-3-00-053387-7